Rock Mech Rock Eng
DOI 10.1007/s00603-017-1261-8

ORIGINAL PAPER

Experimental Investigation of the Effect of Bedding Planes on Hydraulic Fracturing Under True Triaxial Stress

Bingxiang Huang[1] · **Jiangwei Liu**[1]

Received: 4 November 2016 / Accepted: 6 June 2017

Abstract A bedding plane effect occurs when hydraulic fractures encounter the bedding plane. True triaxial hydraulic fracturing experiments were conducted with test blocks containing bedding planes. The effects of bedding plane properties and stress state on fracture propagation were analyzed. When hydraulic fracture encounters the bedding plane in sedimentary stratum, it usually propagates along the bedding plane at first. When the hydraulic pressure increases to a critical value in the direction of main hydraulic fracture, the main hydraulic fracture continues propagating along the original direction. The length of the long axial of the hydraulic fracture propagating along the bedding plane is greater than the length of the main hydraulic fracture before penetrating the bedding plane, and both of them are greater than the length of the main hydraulic fracture after penetrating the bedding plane. Three-dimensional propagation models were established. Three propagation forms of hydraulic fractures existed when encountering bedding planes: (1) propagation along the bedding plane; (2) initial propagation along the bedding plane followed by penetration of the bedding plane and propagation along the principal direction; and (3) direct penetration of the bedding plane and propagation along the principal direction.

Keywords Rock strata bedding plane · Triaxial stress · Hydraulic fractures · Propagation behavior · Bedding plane effect

✉ Bingxiang Huang
huangbingxiang@cumt.edu.cn

[1] State Key Laboratory of Coal Resources and Safe Mining, China University of Mining and Technology, Xuzhou 221116, China

1 Introduction

The control of hard roof, the prevention and treatment of coal and rock burst, gas extraction in coal seams with low permeability and prevention and treatment of coal and gas outburst are technical problems faced in underground coal mining. Transforming the structure of coal and rock masses is the core issue in solving all of these problems. By increasing the number of hydraulic fractures in the coal and rock strata, their strength can be lessened and permeability can be improved (Huang et al. 2011, 2014). Understanding the propagation law of hydraulic fractures and controlling their direction and morphology are premises of successful hydraulic fracturing. The reservoir strata of oil, natural gas and coal are sedimentary formations developed over a long historical period. They all have transverse layered structure. Visible coal–coal, rock–rock or coal–rock planes exist in the coal and rock strata, and these are generally referred to as bedding planes. A bedding plane effect occurs when hydraulic fractures encounter the bedding plane (Blair et al. 1989; Daneshy 1978). Fracture propagation is affected by bedding planes. The study of the effect of bedding planes on fracture propagation helps explain the propagation law of hydraulic fracture around bedding planes and control hydraulic fractures propagating within a specific stratum.

At present, hydraulic fracturing is typically applied in coal seam, oil reservoir and shale bedding. The interest in the use of the method is in coal seams, oil reservoir and shale bedding. On-site survey of the above strata and their roof and floor shows that bedding planes usually close tightly. The surfaces of bedding planes are flat with low roughness. Little filling material exists in the bedding plane. The stratum thickness that contains bedding planes is large. Therefore, the opening, intensity, roughness and filling material properties of the bedding plane are not

Published online: 28 June 2017

considered. Only the adhesive property is taken into consideration in the study of the bedding plane effect. Basic indices of the adhesive property include tensile adhesive strength, bending adhesive strength and shear adhesive strength. The failure mode of hydraulic fracturing is tension destruction. As a result, the tensile strength is considered as the key factor in analyzing the adhesive strength of the bedding plane.

The propagation of hydraulic fracture in the direction perpendicular to the interface is affected by the bedding plane (Fisher and Warpinski 2012; Rutledge et al. 2014). When hydraulic fractures penetrate the bedding plane and propagate perpendicular to the interface, fluid first permeates along the interface, and then hydraulic fractures penetrate the interface perpendicularly (Blair et al. 1989). Hydraulic fractures may penetrate through the bedding plane or propagate along the bedding plane. Whether hydraulic fractures penetrate the bedding plane not only depends on the differences in mechanical properties of the pay zone and interlayer (Biot et al. 1983), but also depends on the interface property, vertical stress difference, horizontal stress difference (Biot et al. 1983; Warpinski et al. 1980, 1982; Anderson 1981; Cleary 1980), fracturing fluid pressure, fracture geometry, filtration effect and other factors (Warpinski et al. 1980; Teufel and Clark 1984). Hydraulic fractures do not penetrate natural fractures unless both the principal stress difference and approach angle are large. In most cases, a hydraulic fracture stops extending or changes its direction when encountering natural fractures (Thiercelin et al. 1987; Blanton 1982, 1986). The effect of bedding plane in shale on the propagation of hydraulic fracture is observed directly in laboratory hydraulic fracturing tests (Suarez-Rivera et al. 2013; Guo et al. 2014; Zou et al. 2016); the existence of bedding plane in shale and the natural fractures create conditions for spatial network structure of hydraulic fractures. Several simple behavior models for hydraulic fracture after encountering bedding plane are obtained through true triaxial experiments, and hydraulic fracture can penetrate the natural fracture if the strength of rock decreases or the strength of the bedding plane increases (Wei et al. 2016). Quantitative research shows that the horizontal stress difference and the angle of approach have great influence on the opening and shear failure mechanism of natural fractures (Zhou et al. 2008, 2010). A complex numerical model of hydraulic fracturing in natural reservoirs was built (Weng 2015). The stress intensity factor of a hydraulic fracture in a layered stratum was calculated (Zhao and Chen 2010; Tada et al. 1973), and criteria for hydraulic fracture penetrating the bedding plane were established (Biot et al. 1983). Criteria for predicting hydraulic fracture behaviors when encountering non-orthogonal natural fractures were also developed (Gu et al. 2011). Criteria for hydraulic fractures penetrating natural fractures in three-dimensional spaces were established (Cheng et al. 2014).

However, in all of the studies mentioned above, the basic extension morphology, conceptual models and behavior characteristics of a hydraulic fracture under bedding plane conditions were not clearly involved. Further research is needed to study these problems.

2 Experimental Program

2.1 Physical and Mechanical Properties of a Bedding Plane Simulated by Cement Mortar

After serious consideration, the cement mortar was chosen to be used to simulate coal and rock, and the reasons are as follows: (1) in oil or shale gas well, there is no channel to enter into the reservoir to conduct sampling, the size of the core sample by drilling is little, and the outcrop is usually weathered. While the sampling can be conducted in the coal mine, (2) it is difficult to sample, cut and transport the test block containing bedding planes. The original conditions of the test block may be affected; (3) affected by the site conditions and differences in physical properties of bedding planes, the discreteness of field sampling is generally large, which has great impact on the experiment results; (4) the mechanical property of cement mortar with fixed material ratio is steady and its discrete is low, which meets the requirements of the experiments. Cement mortar test blocks were used in the experiments to simulate hydraulic fracturing on site. The adhesive strength of the bedding plane was controlled by setting time. To study the craftsmanship of test blocks with a bedding plane, the mechanical properties of the bedding plane were tested. No. 32.5 cement, filtered fine sand and fresh water with a mass ratio of 3.5:1:0.3 were mixed to cast test blocks. Table 1 shows the physical and mechanical parameters of the cement mortar.

To eliminate the influence of temperature and humidity on bedding plane properties, the cement mortar blocks were cast indoors. A steel mold with dimensions of $70 \times 70 \times 70$ mm^3 was used to cast the test block. Figure 1a shows the test block containing a bedding plane. The test block was cast in two steps. The lower layer with height of 35 mm was first cast. After a period of time, the upper layer was cast. The initial setting time of the cement in the experiments was not less than 45 min, and the final setting time was not less than 600 min. Three days after the test block was cast, the compressive strength of the block was not less than 10% of its ultimate compressive strength, and its bending strength was not less than 2.5% of the

Table 1 Physical and mechanical parameters of the cement mortar

Porosity ϕ (%)	Permeability K (mD)	Uniaxial compressive strength σ_c (MPa)	Modulus of elasticity E (GPa)	Tensile strength σ_t (MPa)	Cohesion c (MPa)	Angle of internal friction φ (°)	Fracture toughness K_{1c} (N mm$^{3/2}$)
12.79	1.13	6.27	0.72	1.65	2.54	31.29	13.23

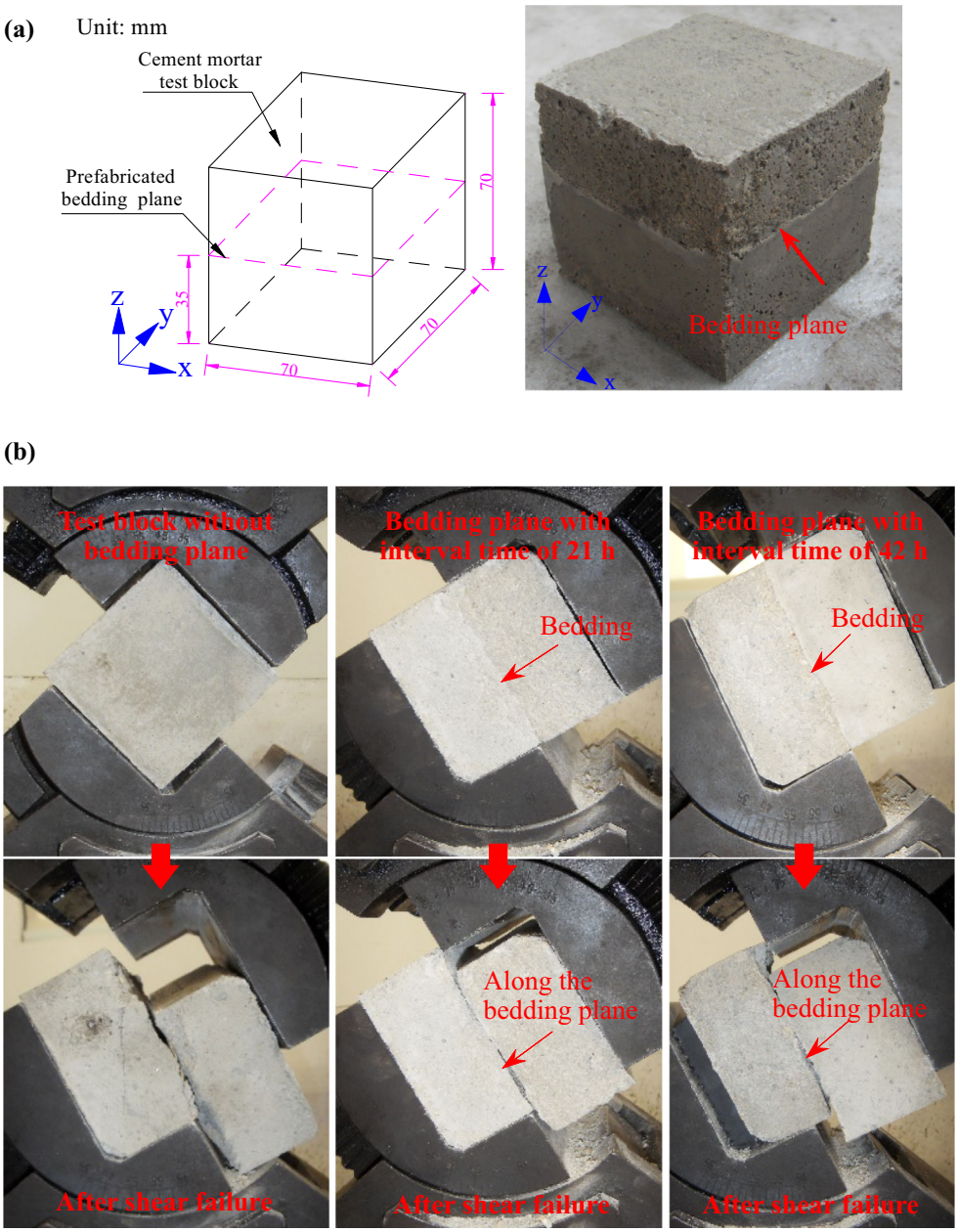

Fig. 1 Mechanical parameters testing of bedding plane. **a** Test block containing a bedding plane for shearing test and **b** failure forms of shear test

ultimate bending strength. Test blocks were cast in three ways. The first test block had no bedding plane. In the casting of the second one, the upper layer was cast 21 h after the lower layer was cast. In the third test block, the interval time between the lower and upper layer was 42 h. Figure 1b shows the shear test results of the test blocks cast in different ways.

Multiple shear failure planes occur in the test block without a bedding plane. No obvious weak plane exists in the test block. The shear failure planes occur along the

Table 2 Mechanical parameters of cement mortar test blocks

Test block type	Cohesive force c (MPa)	Internal friction angle φ (°)	Tensile strength (MPa)
No bedding plane	0.96	37.21	0.95
With interval time of 21 h	0.56	40.98	0.51
With interval time of 42 h	0.30	39.79	0.28

bedding plane in test blocks with a prefabricated bedding plane. The number of associated fractures is also small. A weakening effect of bedding planes exists in the shear experiments. Table 2 shows the tensile strength of the test blocks calculated by the Mohr–Coulomb criterion. The mechanical properties of simulated bedding planes with interval times of 21 and 42 h are similar to typical rock–rock and coal–coal bedding planes, respectively. Therefore, the test blocks can be used to simulate field bedding planes.

2.2 Experimental System

A 500 mm × 500 mm × 500 mm true triaxial hydraulic fracturing experimental system was used in this study (Fig. 2) (Huang et al. 2011, 2014). The experimental system consisted of a bench frame, a loading system and a monitoring system. The true triaxial stress was loaded on cubic test blocks by five to six flat jacks to simulate crustal stress. The size of the cubic block was 300 × 300 × 300 mm^3 or 500 × 500 × 500 mm^3. The pressure from the loading plate in three directions could reach 4000 kN.

The loading of confining pressure and water pressure was controlled by a four-channel electrohydraulic servo control loading system. A MOOG valve was used in the electrohydraulic servo system. The accuracy of servo control was high enough to meet the demand of a pore pressure simulation experiment. Three channels of the electrohydraulic servo were used to control the loading of confining pressure and water pressure. One channel was used to control the oil–water transition supercharger to realize real-time control of water pressure. The loading rate of water pressure could be controlled in two modes: (1) The water pressure increased by a certain value in unit time (MP/min) or (2) the water injection volume increased by a certain value in unit time (mL/min). The loading rate of water pressure could be adjusted stepwise and controlled by computer programs. Pressure sensors and displacement sensors were installed at the rear end of the oil–water loading converter. The servo value was controlled by sensor signals to achieve dynamic loading of water pressure. The water pressure for borehole hydraulic fracturing could reach 63 MPa. During the experiment, triaxial confining stress and the water pressure curve were displayed on the software interface in real time. The experimental data were also recorded. Small copper tube connecting with pressure sensors was used as water injection pipeline to reduce pressure loss and attenuation.

An eight-channel high-frequency acoustic emission (AE) instrument was used to collect the AE signals during the experiment. AE parameters were set as follows: threshold value = 40 dB, preamp gain = 40 dB, lower limit of analog filter = 1 kHz, upper limit of analog filter = 400 kHz and sample frequency = 20 Hz. The name of the sensor is R6. The operating frequency is 35–100 kHz, and the resonance frequency is 55 kHz.

2.3 Preparation of Test Block

Cement mortar blocks with dimensions of 300 × 300 × 300 mm^3 were used to simulate coal and rock layers. Common borehole packers were used to seal the borehole. The external diameter of the borehole packer was 21 mm, the internal diameter was 10 mm, and the length of the borehole packer was 220 mm. Figure 3a shows the preparation process of the test block containing bedding planes. Figure 3b shows the size and structure of the test blocks. Two parallel bedding planes were placed vertically and symmetrically on either side of the borehole. The distance between the bedding plane and the borehole was 68 mm (larger than six times the borehole diameter). The distance between the bedding plane and the boundary surface was 82 mm (larger than 1/6 of the side length). With the structure described above, the effects of the borehole and the border on the hydraulic fracture propagation could be eliminated. The test blocks with three layers and two bedding planes were cast three times (Fig. 3b). Table 3 shows the interval time in casting each layer. The formation process of coal–rock plane was simulated by the interval time in casting the upper and lower layer. The mechanical properties of the bedding plane were also controlled by the interval casting time of different layers. Figure 3b shows the morphology of the bedding plane. The bedding plane with interval casting time of 21 h was used to simulate rock–rock interface. The bedding plane with interval casting time of 42 h was used to simulate coal–coal interface.

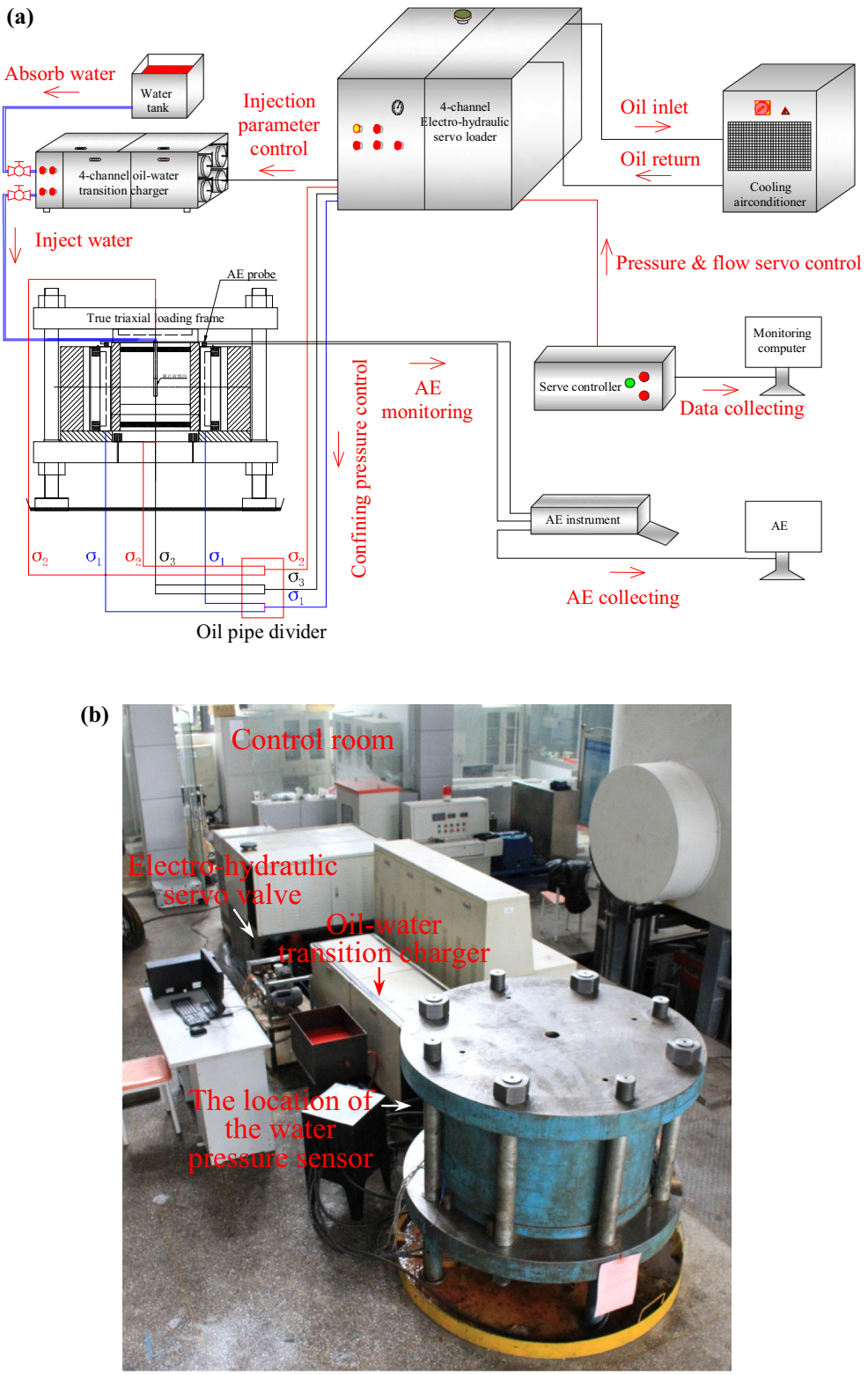

Fig. 2 Experimental system for true triaxial hydraulic fracturing. **a** Block diagram and **b** physical photograph

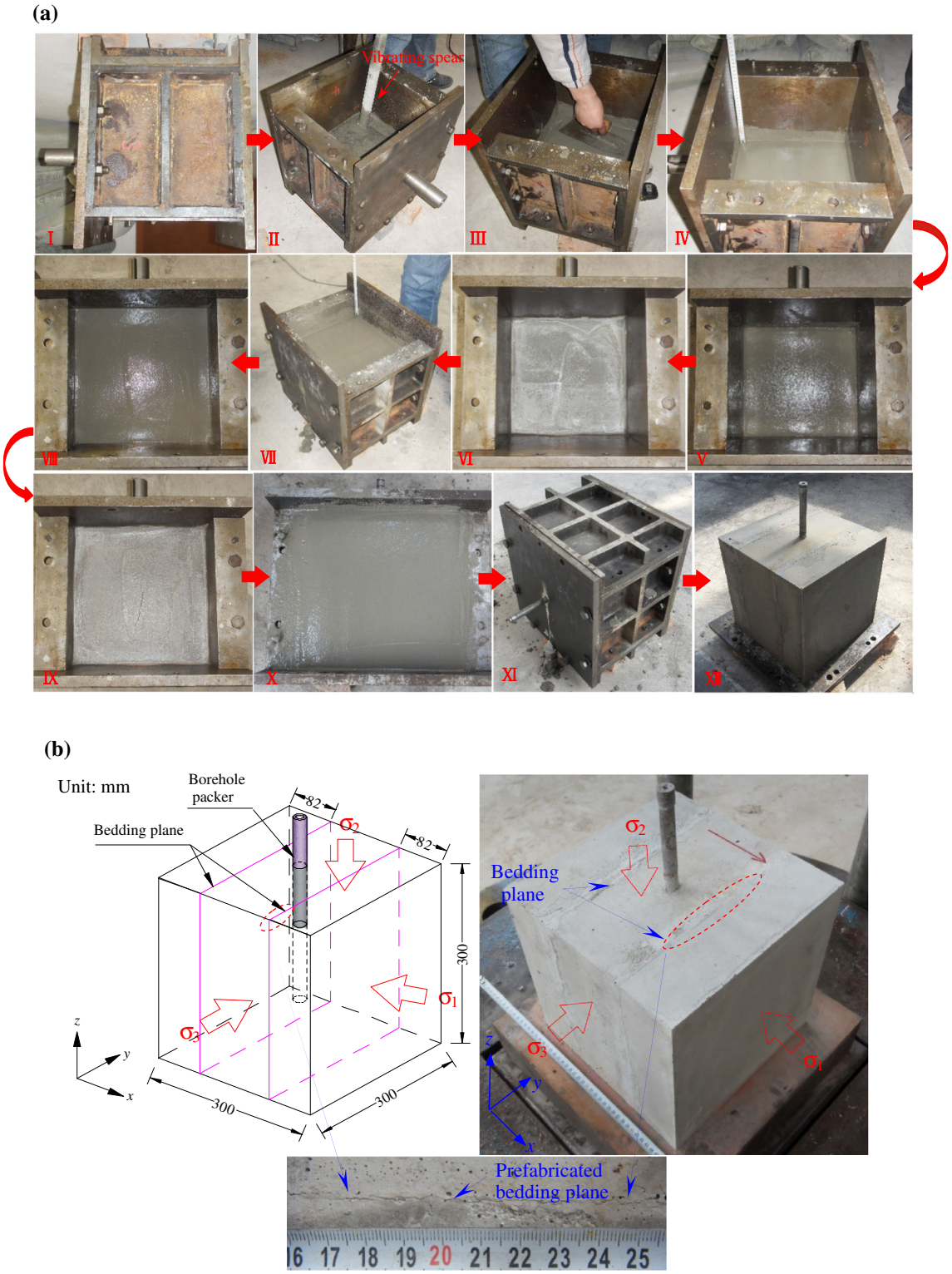

Fig. 3 Production process of the bedding plane and test block of bedding plane containing for hydraulic fracturing. **a** The preparation process of the test block containing bedding planes: *I* putting down for casting, *II* adding cement mortar and vibrating, *III* screeding, *IV* verifying the location of the bedding plane, *V* start air-drying, *VI* after air-drying, *VII* the second bedding plane is finished, *VIII* start air-drying the second bedding plane, *IX* the air-drying of the second bedding plane is finished, *X* the third layer is finished and start air-drying, *XI* the test block is finished, *XII* the upper plate is placed and start air-drying and **b** test block containing bedding planes for hydraulic fracturing

Table 3 Experimental programs of hydraulic fracturing in test blocks with bedding planes

No.	Stress state (MPa)	Principal stress difference $\sigma_1 - \sigma_3$ (MPa)	Interval time (h)
21-1	$\sigma_1 = 6$; $\sigma_2 = 5.5$; $\sigma_3 = 5$	1	21
21-2	$\sigma_1 = 3$; $\sigma_2 = 2.75$; $\sigma_3 = 2$	1	21
42-1	$\sigma_1 = 6$; $\sigma_2 = 5.5$; $\sigma_3 = 3$	3	42
42-2	$\sigma_1 = 6$; $\sigma_2 = 5.5$; $\sigma_3 = 4$	2	42

2.4 Experimental Method

The six boundary surfaces of the test block contacted directly with the steel plates. Then, the confining stress was loaded on the steel plates by flat jacks. The typical stress state in a coal mine site was simulated (Table 3). Four groups of two-factor experiments were conducted. The stress state and the interval casting time were different between any two groups. To simulate large-flow hydraulic fracturing and eliminate the effect of time, the flow rate was set at 500 mL/min. Red poster dye was added to the water tank to show the fracture propagation track.

The test block was placed in the true triaxial stress loading framework, and the AE sensors were fixed. The controller was turned on to load confining stress. When the confining pressure reached the target value, it was held stable for 3 min.

3 Water Pressure and AE Signals During Hydraulic Fracturing Experiments

As a control, a typical hydraulic fracturing experiment was conducted using a test block without a bedding plane. The confining stresses were $\sigma_1 = 12.31$ MPa, $\sigma_2 = 7.69$ MPa and $\sigma_3 = 3.08$ MPa, and the water output volume was set to 100 mL/min. Because the rock is porous medium, the permeation and leak-off exist during the initiation and propagation of the hydraulic fractures. When the flow rate is smaller, with the continuous injection of the water, the water pressure gradually increases; when it reaches the breaking condition, the cracks propagate; then the liquid storing space in the block is larger, which results in the decrease in the water pressure, and the crack temporarily stops extension. Then, with the continuous injection of the water, the water pressure gradually increases to a certain degree again and the crack continues to extend again. As a consequence, periodic increase and decrease in water pressure may be noticed from the water pressure curve (Fig. 4a). One cycle of increase and decrease in water pressure indicated that the hydraulic fractures to extend for one time. With injecting water into the test block, the water pressure increased gradually (Cheng 2012).

Figure 4b, c shows water pressure and AE signals during the hydraulic fracturing. The total experimental process can be divided into three stages: (1) water injection and pressure increase (AB); (2) initiation and propagation of hydraulic fractures (BF); and (3) hydraulic fractures connecting with the boundary surface and water pressure decreases (FG). Before the initiation of hydraulic fracture, the AE signals are weak in the pressure increase stage (AB). Nine water wave peaks occur during the fracture stages (BF), and nine obvious AE events and energies are also monitored by the AE monitoring equipment. An accurate correspondence of the time of water pressure wave peaks and the monitored AE signals peaks occur, indicating the periodic propagation of hydraulic fracture during the fracture state. During the fracture stages (BF), initial fracture stage (BC) and steady fracture stages (CF) will occur. The water pressure in the initial fracture (point B) is the maximum. The water pressure decrease (BC) after fracture is also the maximum, and the corresponding AE signals are also the strongest. In steady fracture stages (CF), the water pressure as well as the corresponding AE signals fluctuates periodically. At the time the water pressure decreases sharply, the AE events and energies are the strongest. The obvious correspondence between the water pressure and the AE signals indicates the process of "fracturing at high water pressure–dilatation and water pressure decrease–water pressure increase and refracture". After hydraulic fracture propagating to the surface of the test block, during the water decrease (FG) stage, the water pressure decreases gradually, and the AE signals also gradually decrease to zero.

Comparison of Fig. 4a–c indicates that in the stable propagation stage (CF), both the peak water pressure and the fluctuation amplitude increase first and then decrease. During the CD stage, the peak water pressure, fluctuation amplitude and AE signals gradually increase. The water pressure drop reaches the maximum during the DE stage, showing that hydraulic fractures encounter the bedding plane. During the EF stage, the peak water pressure, fluctuation amplitude and AE signals decrease gradually. Hydraulic fractures initiate from the borehole wall. With the increase in the extension range, the water pressure drop increases gradually during and after the propagation process. The released energy is also enhanced. After

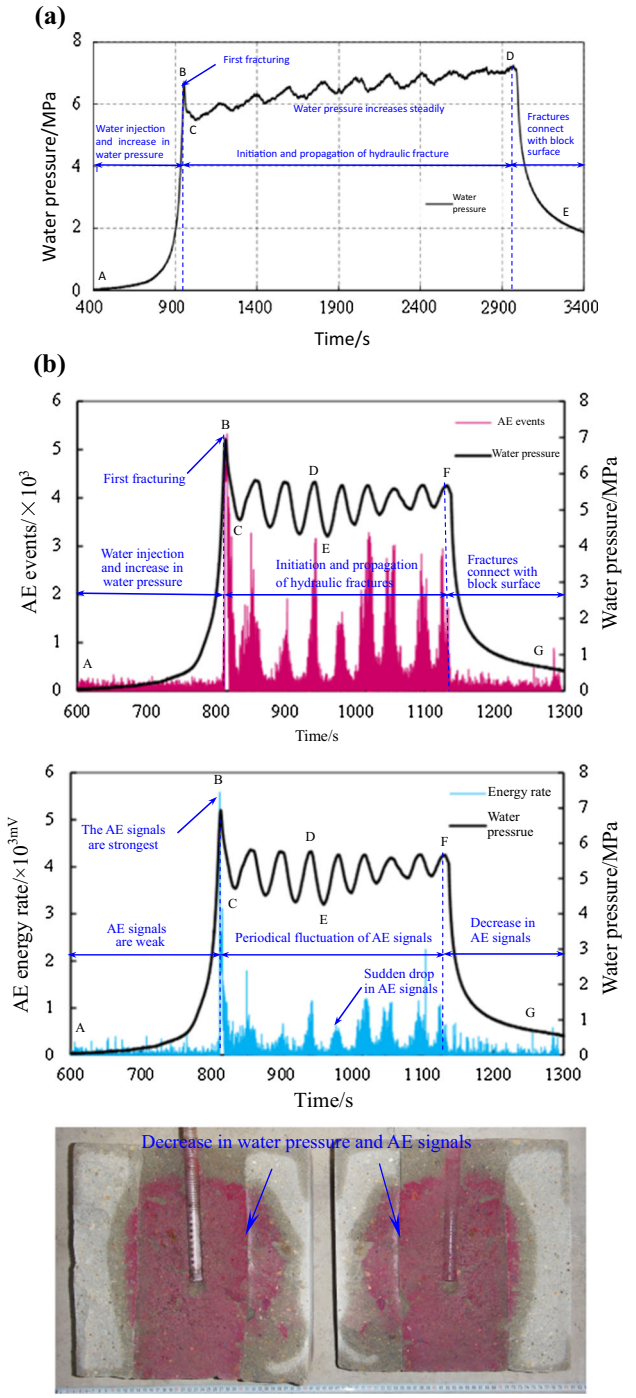

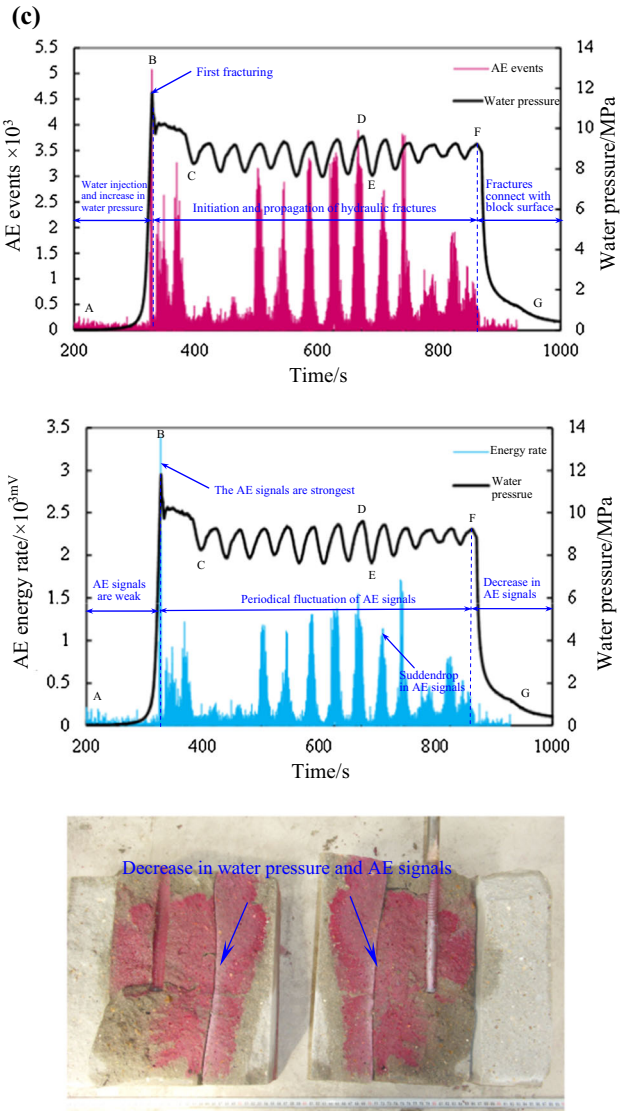

Fig. 4 Hydraulic pressure and AE characteristic in the hydraulic fracturing process. **a** Test block without a bedding plane, **b** test block containing bedding plane (test block 42-1) and **c** test block containing bedding plane (test block 42-2)

Fig. 4 continued

hydraulic fractures encounter the bedding plane, high-pressure water flows into the fracture space. After that, the fracture propagation behaviors tend to be steadily affected by propagation along the bedding plane.

4 Basic Propagation Law of Hydraulic Fractures Around a Bedding Plane

4.1 Effect of a Bedding Plane

The main hydraulic fracture initiates from the borehole wall and then propagates along the direction perpendicular to σ_3. Figure 5a shows the main fracture surface of the test block without a bedding plane. In test blocks with bedding planes, however, two extension types may occur when hydraulic fractures encounter the bedding plane: continuous extension and discontinuous extension (Fig. 5b). Continuous extension means that the edge of the hydraulic fracture is a continuous circular arc despite the existence of the bedding plane. The bedding plane has almost no effect on the extension direction of the hydraulic fracture. In

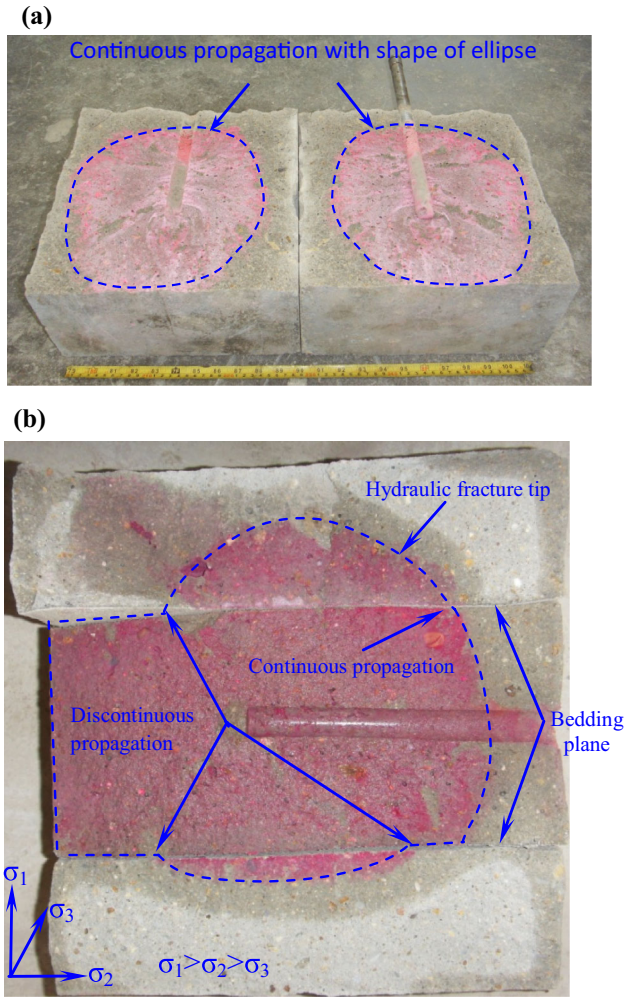

Fig. 5 Extension form of hydraulic cracks. **a** Test block without bedding plane and **b** test block containing bedding planes

discontinuous extension, the fracture front is not consistent, and an obvious difference in intensity of the dye color exists on the two sides of the bedding plane. After hydraulic fractures encounter the bedding plane, they extend along both the bedding plane and the principal direction (the direction perpendicular to σ_3). When hydraulic fracture encounters the bedding plane, two types of hydraulic fractures will occur, i.e., hydraulic fracture propagating along the bedding plane or penetrating it. To distinguish them, concepts of "main hydraulic fracture," "bedding plane fracture" and "wing hydraulic fractures" are explained. The bedding plane fracture means the hydraulic fracture propagates in the bedding plane and along the direction of bedding plane. When the rock is homogeneous around the bending plane, one main hydraulic fracture will generate in rock strata, which is called "main hydraulic fracture"; while if the natural fissures exist in the rock around the bedding plane, hydraulic fractures will generate at the tip of the natural fissures,

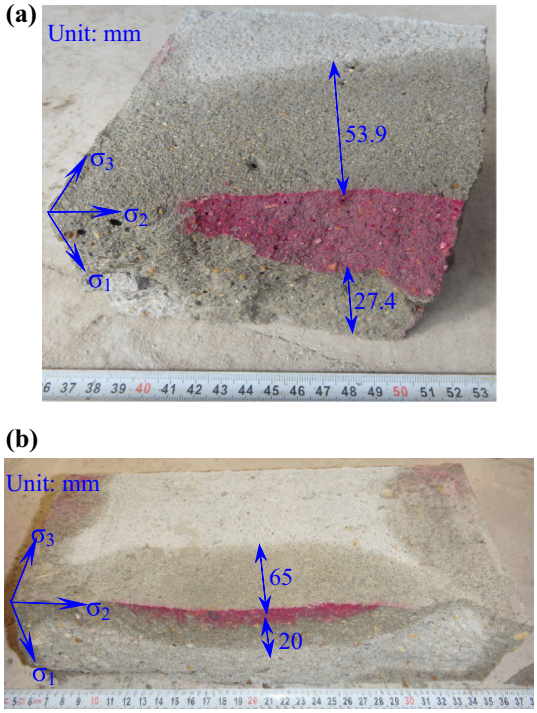

Fig. 6 Characters of the permeating region around the bedding plane. **a** Test block 21-1 and **b** test block 42-1

which are called "wing hydraulic fractures." In the bedding plane, hydraulic fractures extend in the shape of an ellipse. With the extension of the major axis of the fracture surface, the water pressure loss increases within hydraulic fractures. As a result, the water pressure at the orifice increases. If water pressure increases to the critical breakdown pressure in the principal stress direction, hydraulic fractures penetrate the bedding plane. Along the bedding plane, the water pressure gradient needed to extend the fracture is low. It is easier for the main hydraulic fracture to propagate along the bedding plane than along σ_1. As a result, the propagation rate and range of main fractures in the bedding plane are larger than along σ_1. The propagation along the principal direction (the direction of σ_1) is discontinuous.

The normal stress σ_1 must be overcome if hydraulic fractures propagate along the bedding plane. Similarly, normal stress σ_3 must be overcome when hydraulic fractures propagate along the direction of σ_1. A larger normal stress has to be overcome when hydraulic fractures propagate along the bedding plane because σ_1 is larger than σ_3. However, the width of the water stain along the bedding plane is 1.97–2.17 times that of the water stain along the σ_1 direction (Fig. 6). Compared to rock, the permeability of the bedding plane is higher, and the fracture water pressure is lower. Hydraulic fractures extend more easily along bedding planes. A large area of water stain in a bedding plane indicates the opening of the bedding plane. No dye

color in the bedding plane indicates that the opening of the bedding plane is small and dye particles cannot enter into the bedding plane.

The bedding plane effect prevents the hydraulic fractures from extending along the principal direction and prompts the hydraulic fractures to extend along the bedding plane. Because of the bedding effect, discontinuous propagation of fractures occurs, and an obvious difference between two sides of the bedding plane can be seen. The hydraulic fractures propagate more easily along the bedding plane if the bedding effect is stronger.

4.2 Spatial Morphology of Hydraulic Fractures Near a Bedding Plane

Hydraulic fractures initiate from the wall of borehole and propagate along the direction perpendicular to the minimum principal stress σ_3 (Fig. 7). Compared to typical ellipse-shaped hydraulic fractures (Fig. 5a), the main hydraulic fracture of a test block with bedding planes (Fig. 8a, b) extends approximately in the shape of an ellipse. The direction of the longer axis of the ellipse is the same as σ_2. Contrasting Fig. 8a, b shows that the stronger the adhesive strength, the less obvious the bedding plane effect. The length of the intersection part of the main hydraulic fracture and fracture along the bedding plane is larger than that of the main hydraulic fracture after penetrating the bedding plane (Fig. 7). The long axial length of

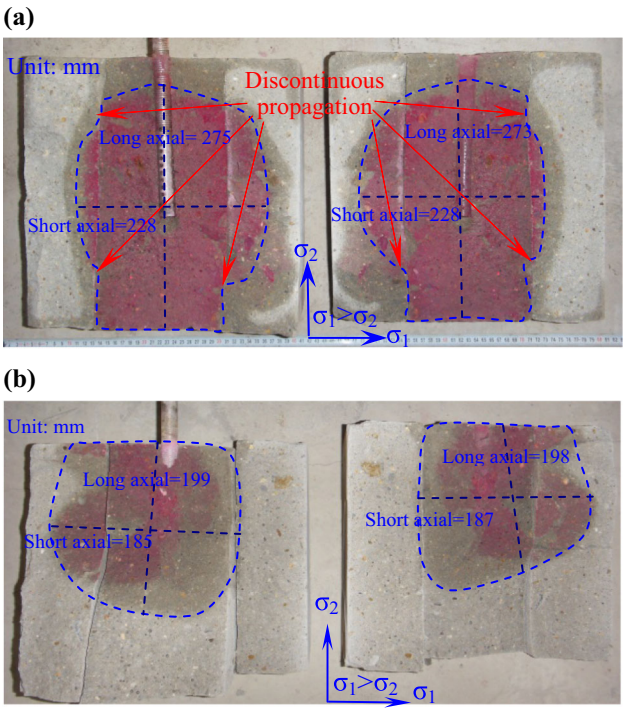

Fig. 7 Characters of the permeating region around the bedding plane. **a** Test block 42-1 and **b** test block 21-2

Fig. 8 Basic morphology of hydraulic fractures near a bedding plane. ▶ **a** Propagation form of hydraulic fractures in bedding plane, **b** distribution characteristics of the permeating region around the bedding plane and **c** schematic diagram of the length relationship between the hydraulic fractures near a bedding plane

fracture along the bedding plane is larger than that of the intersection part (Fig. 8).

A single hydraulic fracture occurs in the bedding plane after hydraulic fractures encounter the bedding plane. The water stains are spheroidal with narrow ends and wide middle forms (Fig. 8a), indicating that the hydraulic fracture extends in the shape of an ellipse. This is the basic propagation form of hydraulic fractures in a bedding plane. The longer axis of the ellipse is perpendicular to σ_3. If the stress state is changed, two or more hydraulic fractures occur approximately along the same direction (Fig. 8a). Multiple hydraulic fractures with irregular shapes may even occur with changed stress state. Cross-fractures and fracture bifurcations also exist (Fig. 8a). Superposition of multiple elliptical water stains results in the irregular water stain around multiple hydraulic fractures.

A permeating zone with a certain width exists around the hydraulic fractures. Ellipse-shaped permeating zones exist around the elliptical fracture surface. The ellipsoidal permeating zone extends along the bedding plane (Fig. 8b).

The general spatial morphology of hydraulic fractures is like the shape of two parallel ellipses intersecting with a hydraulic fracture surface (Fig. 8c). The relation between the lengths of three types of hydraulic fracture around the bedding plane is as follows: length of the long axial of the hydraulic fracture propagating along the bedding plane > length of the main hydraulic fracture before penetrating the bedding plane > length of the main hydraulic fracture after penetrating the bedding plane.

4.3 Three Propagation Forms of Hydraulic Fractures

Three basic propagation forms of hydraulic fractures exist in hydraulic fracturing with bedding planes: (1) Hydraulic fractures propagate along the bedding plane, (2) hydraulic fractures first propagate along the bedding plane and then penetrate the bedding plane and (3) hydraulic fractures penetrate the bedding plane directly and continue propagating along the principal direction. In the first propagation form (Fig. 9a), no fracture penetrates the bedding plane. The water stain range is large. The bedding plane opens obviously, indicating that hydraulic fractures propagate along the bedding plane after they encounter it. In the second form (Figs. 7a, 9b), the main hydraulic fracture penetrates the bedding plane, but the propagation is

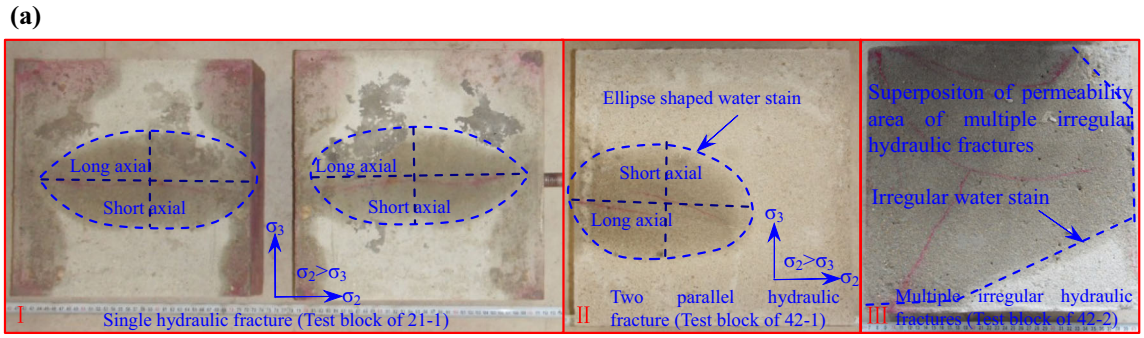
(a)
Long axial
Short axial
Long axial
Short axial
σ3
σ2>σ3
σ2
I
Single hydraulic fracture (Test block of 21-1)
Ellipse shaped water stain
Short axial
Long axial
σ3
σ2>σ3
σ2
II
Two parallel hydraulic fracture (Test block of 42-1)
Superpositon of permeability area of multiple irregular hydraulic fractures
Irregular water stain
III
Multiple irregular hydraulic fractures (Test block of 42-2)

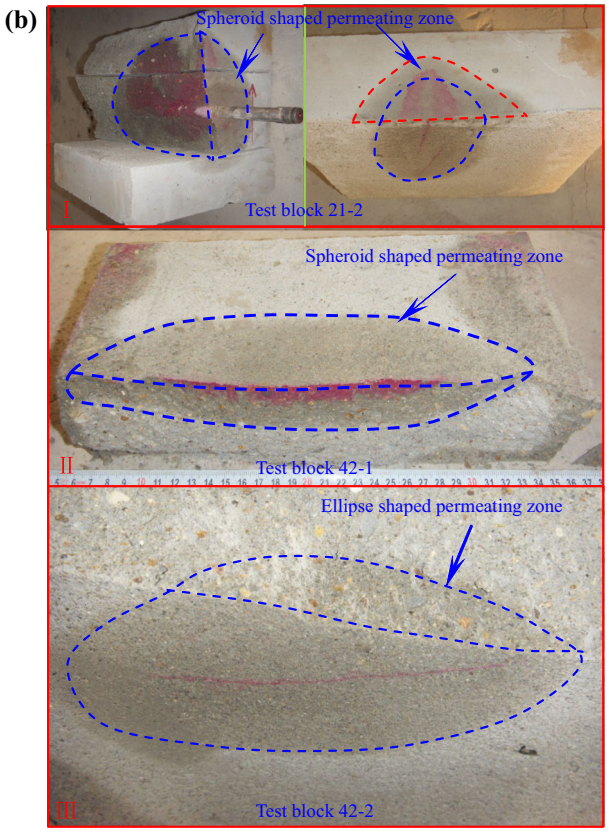
(b)
Spheroid shaped permeating zone
I
Test block 21-2
Spheroid shaped permeating zone
II
Test block 42-1
Ellipse shaped permeating zone
III
Test block 42-2

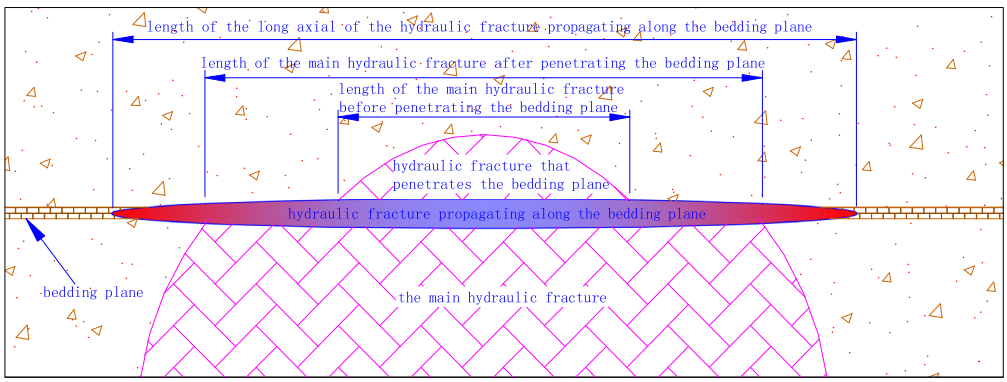
(c)
length of the long axial of the hydraulic fracture propagating along the bedding plane
length of the main hydraulic fracture after penetrating the bedding plane
length of the main hydraulic fracture before penetrating the bedding plane
hydraulic fracture that penetrates the bedding plane
hydraulic fracture propagating along the bedding plane
bedding plane
the main hydraulic fracture

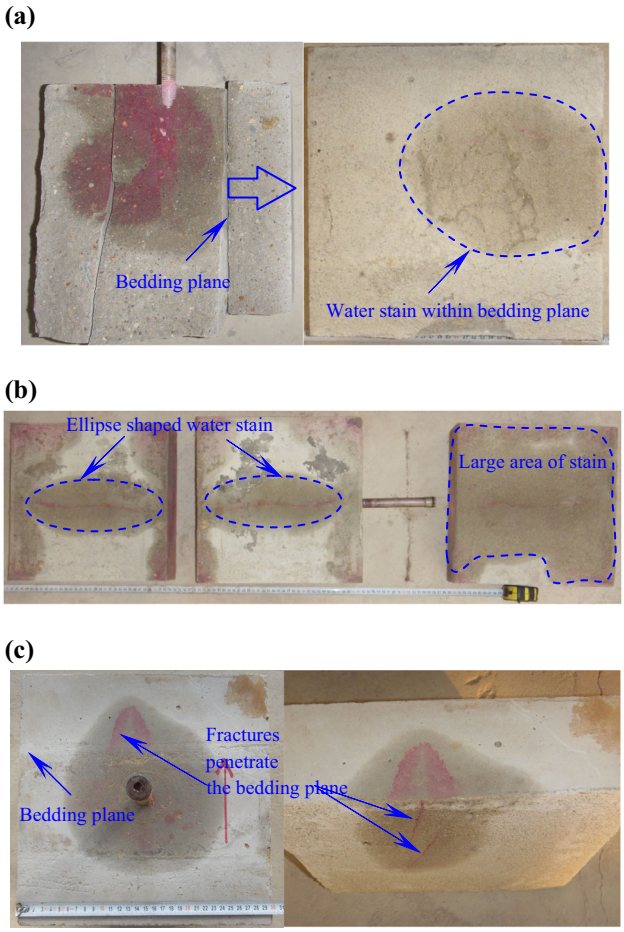

Fig. 9 Three forms of hydraulic crack extension under the impact of the bedding plane. **a** Form I, **b** Form II and **c** Form III

discontinuous. The water stain around the main fracture in the bedding plane indicates that hydraulic fractures propagate along the bedding plane after encountering the bedding plane. With an increase in the water pressure loss, the water pressure at the orifice increases. When the water pressure increases to the breakdown pressure of the rock, hydraulic fractures penetrate the bedding plane and extend along the principal direction. In the third form (Fig. 9c), one or more hydraulic fractures penetrate the bedding plane and continue propagating along the principal direction. The fractures are continuous when penetrating the bedding plane, and their morphology is not affected by the bedding plane. The water stain within the bedding plane is not large (Fig. 9c1). Contrasting Fig. 9c1, c2 shows that hydraulic

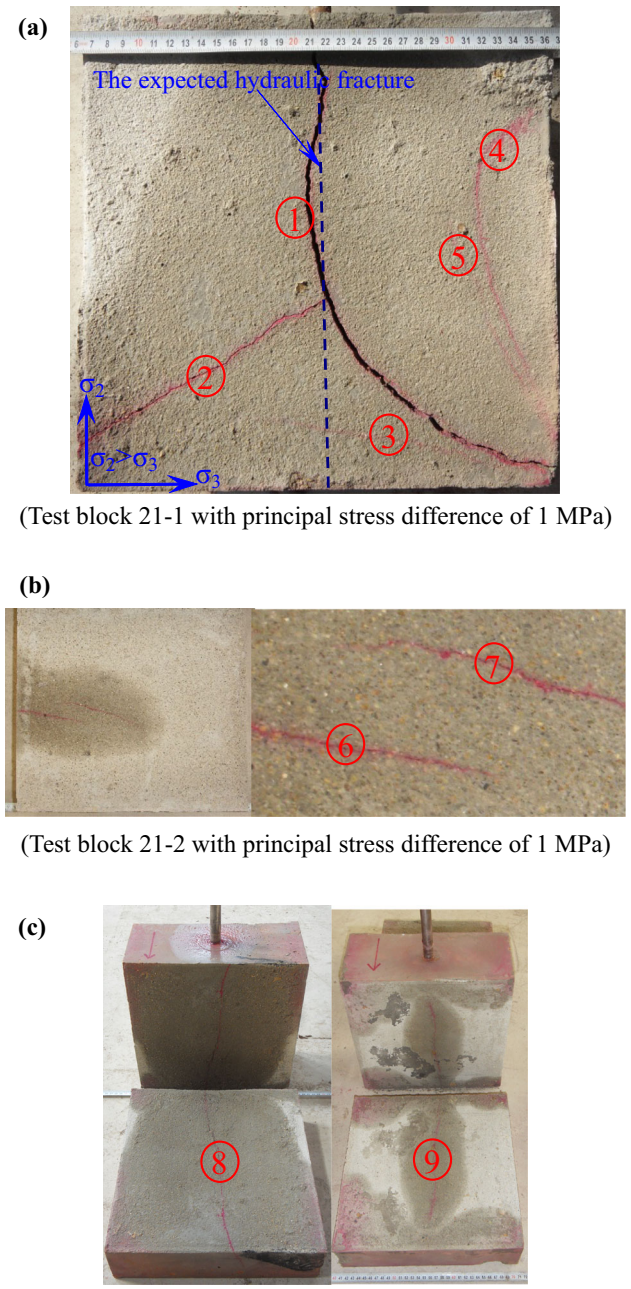

Fig. 10 Basic morphology of hydraulic fractures around bedding plane under different principal stress differences. **a** Multiple irregular hydraulic fractures, **b** two parallel hydraulic fractures and **c** single hydraulic fractures

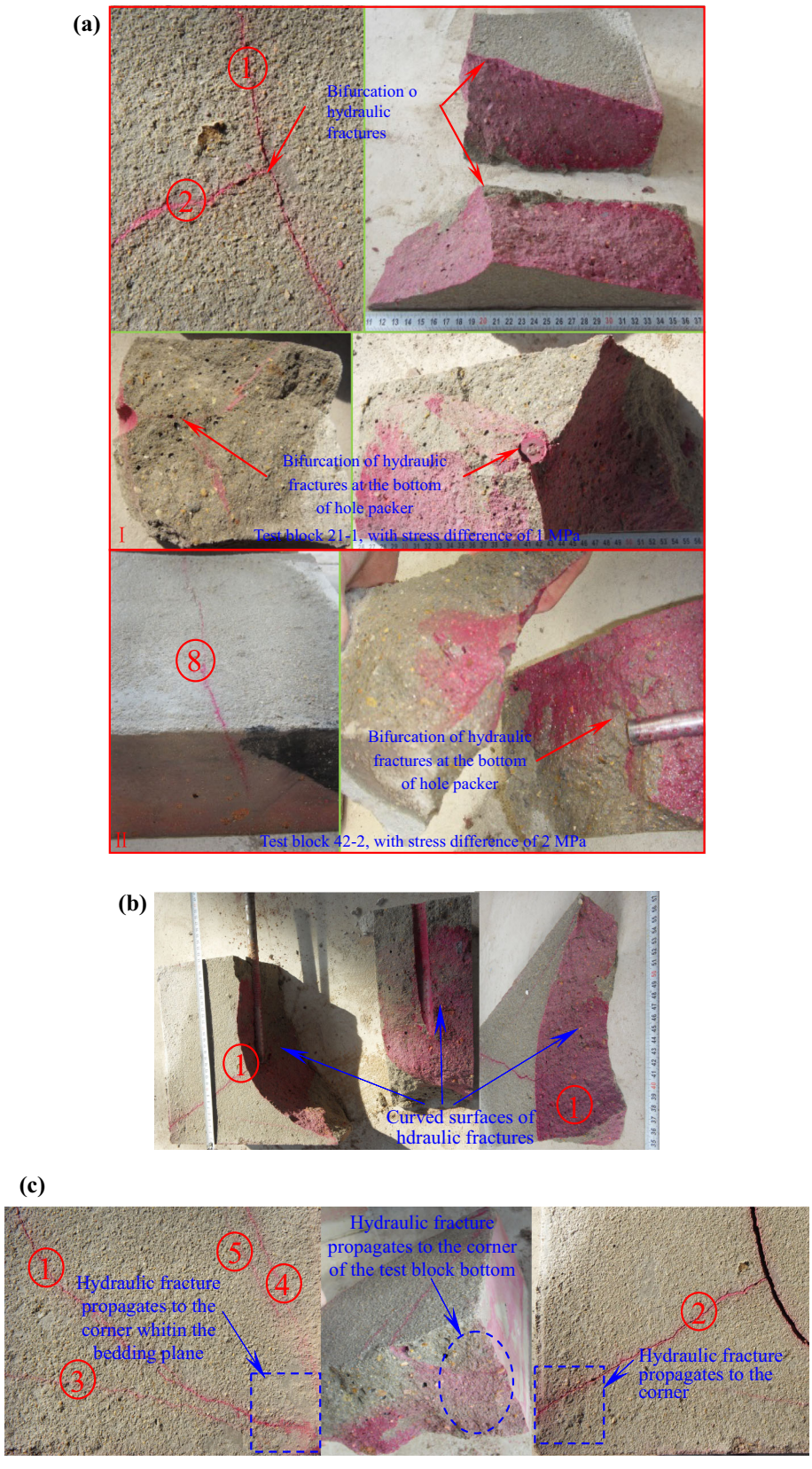

Fig. 11 Reorientation and corner concentration effect of hydraulic fractures. **a** Furcation of hydraulic fractures, **b** reorientation of hydraulic fractures and **c** concentrated fractures at the block corner

fractures are more likely to penetrate a bedding plane with stronger cohesive strength.

5 The Effect of Principal Stress Difference on Hydraulic Fractures

Under different stress states and different bedding plane tensile strengths, the main hydraulic fracture usually propagates along the direction of the maximum principal stress σ_3 (Fig. 10). When the principal stress difference is 1 MPa, five irregular hydraulic fractures occur (Fig. 10a). The main hydraulic fractures ① and ② do not propagate along the predicted direction. When the principal stress difference increases to 2 MPa, two parallel hydraulic fractures occur (Fig. 10b). The angle between the hydraulic fractures and the direction perpendicular to σ_3 is approximately 20°. When the principal stress difference increases to 3–4 MPa, a single fracture occurs at the bedding plane, and the fracture is approximately perpendicular to σ_3. Therefore, with the increase in principal stress difference, the number of hydraulic fractures decreases to one, and the propagation direction of hydraulic fractures tends to be perpendicular to σ_3. The surface of the hydraulic fractures tends to be flat. The distribution of hydraulic fractures tends to be regular, and the propagation direction tends to be determinate.

Fracture bifurcation occurs in hydraulic fracture propagation (Fig. 11a), especially at the bottom of the borehole packer. When the principal stress difference is 1 or 2 MPa, fracture furcation occurs at the bottom of the borehole packer. Fracture furcation even occurs at the bedding plane when the principal stress difference is 1 MPa. No fracture furcation occurs in the test block with a principal stress

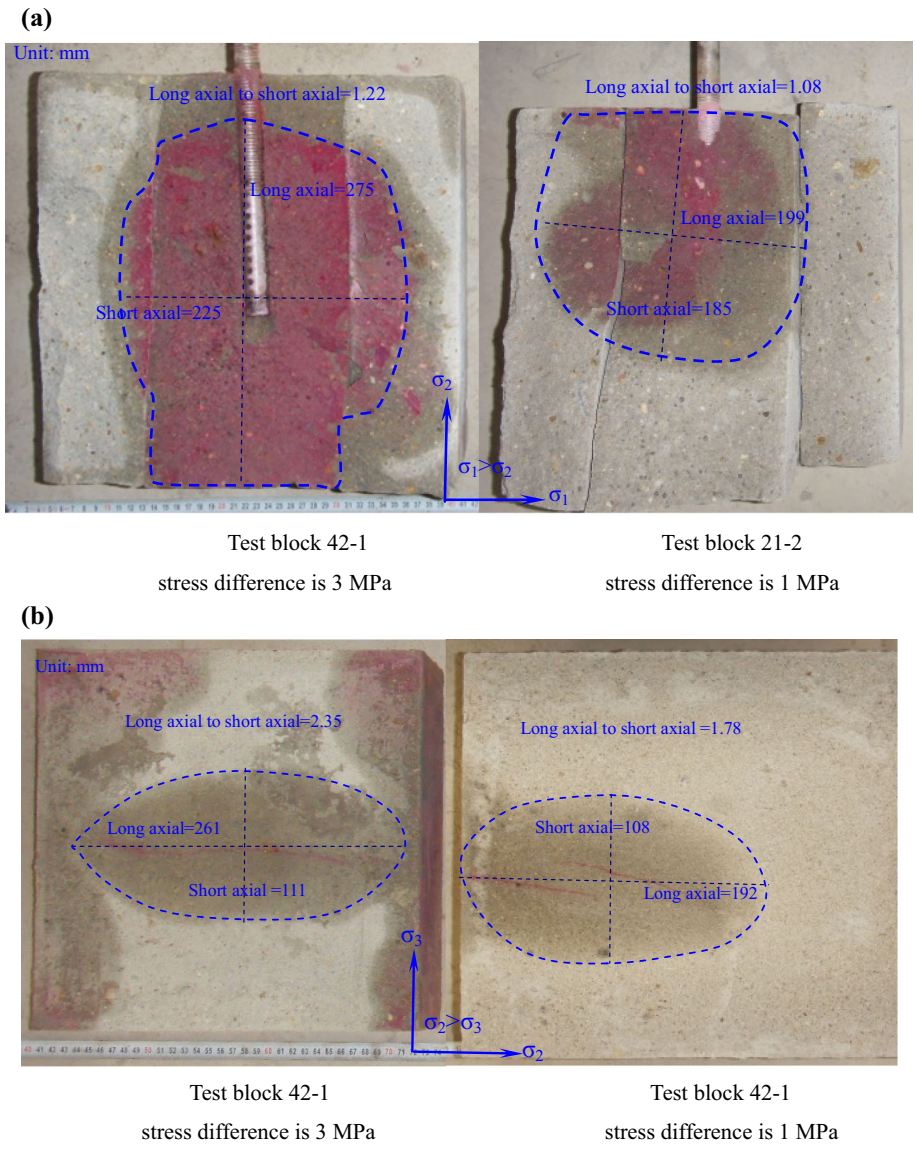

Fig. 12 The effect of principal stress difference on hydraulic fracturing morphology. **a** Ellipse-shaped hydraulic fracture along principal direction and **b** ellipse-shaped hydraulic fracture within the bedding plane

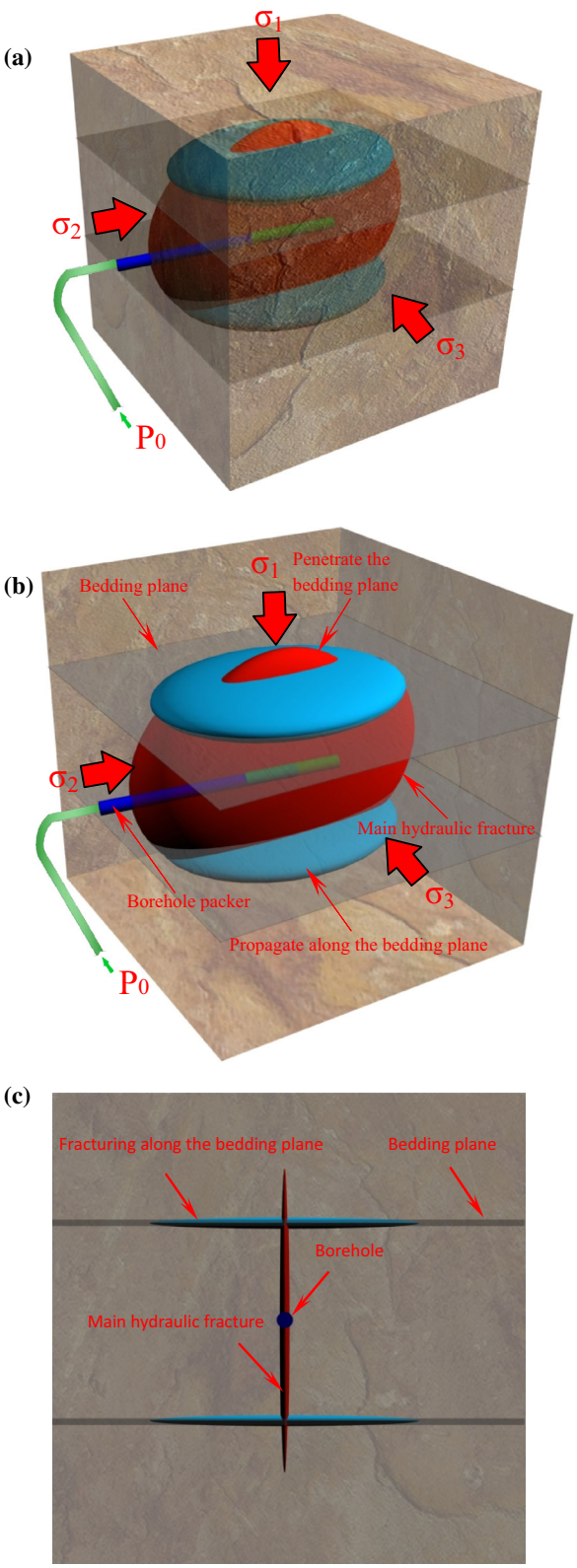

Fig. 13 Conceptual model of the effect of bedding planes on hydraulic fracturing. **a** General view, **b** section view, **c** view in direction of σ_2 and **d** view in direction of σ_3

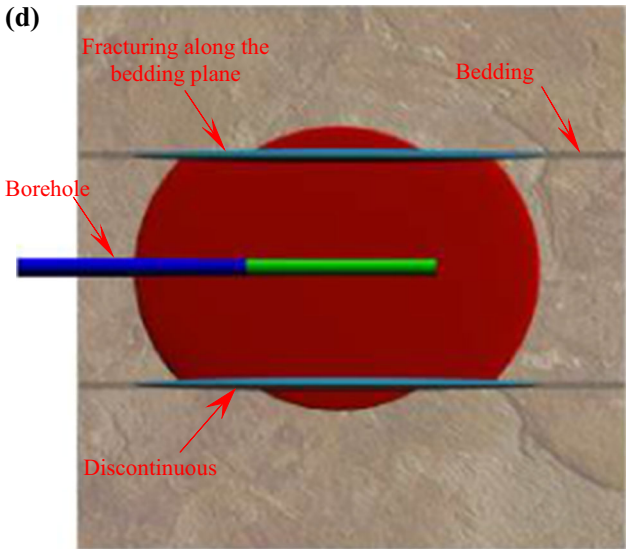

Fig. 13 continued

difference of 2 MPa. Fracture furcation is likely to occur if the principal stress difference is small. The bedding plane has no effect on the morphology of the main hydraulic fracture.

Hydraulic fracture reorientation occurs, and curved fracture surfaces form if the principal stress difference is small (Fig. 11b). Figure 8a shows that the reorientations of fractures ①, ④ and ⑤ are similar. However, the curvature of fracture ① is larger than that of ④ and ⑤. Figure 11b shows that fractures ①, ③, ④ and ⑤ gradually concentrate at one corner of the test block. The distances between fractures ①, ③, ④ and ⑤ decrease as they approach the corner. Fracture ② extends to another corner of the block, indicating that reoriented fractures and furcation fractures also propagate to the block corner. Concentrated fractures at the block corner also occur in the bedding plane and on the block bottom (Fig. 11c). The friction within loading jacks and block surfaces results in stress concentration at the block corner. The concentrated fractures at the block corner are caused by stress concentration mentioned above.

When the principal stress difference is small, the hydraulic fracture surface along the principal direction has the shape of a circle (Fig. 12a). With the increase in principal stress difference, the hydraulic fracture surface along the principal direction has the shape of an ellipse with sharp ends and a narrow middle. The ellipse-shaped hydraulic fracture within the bedding plane is also compressed to be narrow and sharp (Fig. 12b). As a result, with an increase in the principal stress difference, the ellipse-shaped hydraulic fractures along both the principal direction and the bedding plane tend to be narrow and sharp.

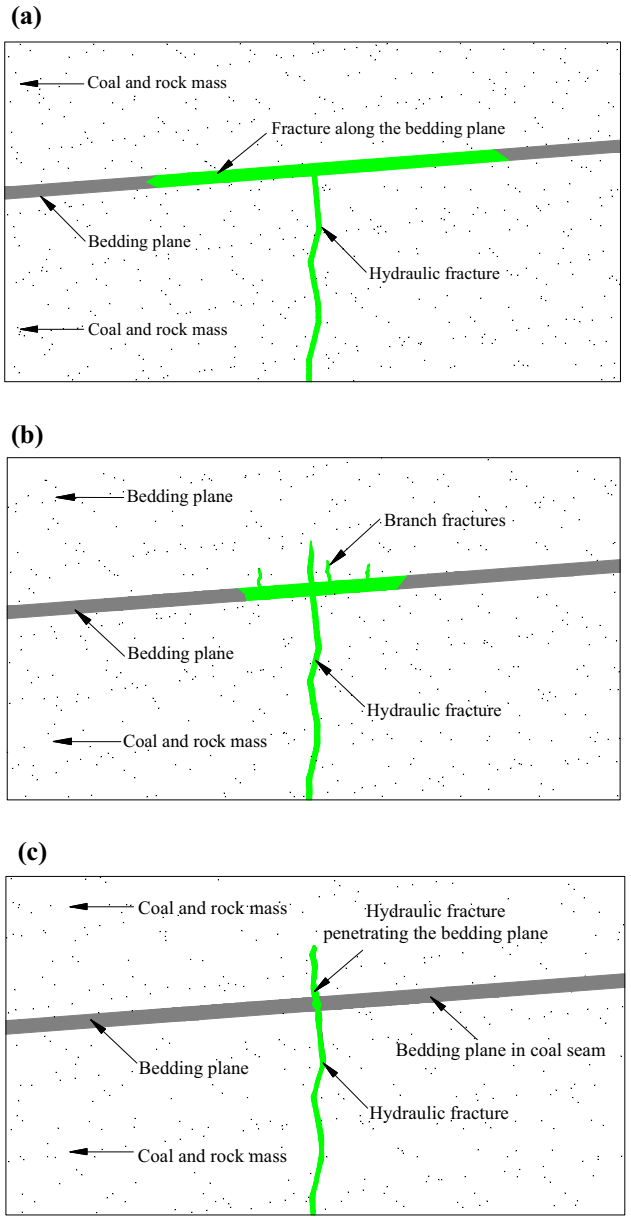

Fig. 14 Conceptual models for the effect of bedding plane on hydraulic fracturing. **a** Model I, **b** Model II and **c** Model III

6 Conceptual Models

The basic propagation law of hydraulic fractures near bedding planes is studied using true triaxial hydraulic fracturing experiments. Based on this, three-dimensional propagation models around bedding planes in sedimentary strata are established (Fig. 13). With the increase in principal stress difference and tensile strength of the bedding plane, three propagation models of hydraulic fractures occur. Model I is that hydraulic fractures propagate along the bedding plane (Fig. 14a). Model II is that hydraulic fractures first propagate along the bedding plane and then penetrate the bedding plane and extend along the principal direction. With an increase in the water pressure loss, the water pressure at the orifice increases. When the water pressure increases to the breakdown pressure in the principal direction, hydraulic fractures continue to extend along the principal direction (Fig. 14b). Model III is that hydraulic fractures penetrate the bedding plane directly and continue to propagate along the principal direction. The extension of hydraulic fractures along bedding planes is not obvious. The fracture morphology is continuous. The fracture propagation is not affected by the bedding plane (Fig. 14c).

7 Conclusions

1. The water pressure and intensity of the AE signals decrease when hydraulic fractures encounter the bedding plane. After this, affected by the bedding plane, the general propagation behaviors of hydraulic fractures tend to be steady.
2. When hydraulic fracture encounters the bedding plane in sedimentary stratum, it usually propagates along the bedding plane at first. When the hydraulic pressure increases to a critical value in the direction of main hydraulic fracture, the main hydraulic fracture continues propagating along the principal direction. The fracture length along the bedding plane is larger than that of the intersection part of the main hydraulic fracture and fracture along the bedding plane. The length of the intersection part is larger than that of the main hydraulic fracture after penetrating the bedding plane.
3. The bedding plane effect may occur and prevent hydraulic fractures from propagating along the principal direction. Affected by the bedding plane effect, the main hydraulic fracture is discontinuous at the bedding plane. Obvious differences in the hydraulic fracture surface exist on two sides of the bedding plane.
4. A single hydraulic fracture forms along the bedding plane after hydraulic fractures encounter a bedding plane, and a spheroidal water stain with wide middle and narrow ends forms. This is the basic propagation form of hydraulic fracture in a bedding plane. A permeating area with a certain width exists around the hydraulic fracture, and a spheroidally shaped permeability area exists around the spheroidally shaped fracture surface. The spheroidal permeating area extends along the bedding plane. The length of the long axial of the hydraulic fracture propagating along the bedding plane is greater than the length of the main hydraulic fracture before penetrating the bedding plane, and both of them are greater than the length of the main hydraulic fracture after penetrating the bedding plane.

5. With an increase in the principal stress difference, the number of hydraulic fractures decreases to 1, and the hydraulic fracture propagation direction gradually turns to the σ_3 direction. The hydraulic fracture surface tends to be flat, and the distribution of hydraulic fractures tends to be regular. The ellipse-shaped hydraulic fractures along the principal direction and the bedding plane tend to be flat and sharp. With a decrease in the principal stress difference, fracture furcation and reorientation occur, and curved hydraulic fracture surface forms.
6. The bedding plane effect decreases with the increase in bedding plane cohesive strength, and the hydraulic fractures are more likely to penetrate the bedding plane.
7. The basic propagation law of hydraulic fractures near bedding planes is revealed through true triaxial hydraulic fracturing experiments. Based on this work, three-dimensional fracture propagation models around bedding planes in sedimentary strata are established. Three basic behavior models of hydraulic fractures exist when encountering a bedding plane: (1) Hydraulic fractures propagate along the bedding plane, (2) hydraulic fractures first propagate along the bedding plane and then penetrate the bedding plane and propagate along the principal direction and (3) hydraulic fractures penetrate the bedding plane directly and propagate along the principal direction.

Acknowledgements Financial support for this work, provided by the National Science Fund for Excellent Young Scholars (No. 51522406), the Fundamental Research Funds for the Central Universities (China University of Mining and Technology) (No. 2014YC03) and the Priority Academic Program Development of Jiangsu Higher Education Institutions, is gratefully acknowledged.

References

Anderson GD (1981) Effects of friction on hydraulic fracture growth near unbonded interfaces in rocks. Soc Pet Eng J 21:21–29

Biot MA, Medlin WL, Masse L (1983) Fracture penetration through an interface. Soc Pet Eng J 23:857–869

Blair SC, Thorpe RK, Heuze FE et al (1989) Laboratory observations of the effect of geological discontinuities on hydrofracture propagation. In: Proceedings of the 30th US symposium on rock mechanics, Morgantown

Blanton TL (1982) An experimental study of interaction between hydraulically induced and pre-existing fractures. In: Proceedings of SPE unconventional gas recovery symposium, Society of Petroleum Engineers

Blanton TL (1986) Propagation of hydraulically and dynamically induced fractures in naturally fractured reservoirs. In: Proceedings of SPE unconventional gas technology symposium, Society of Petroleum Engineers

Cheng QY (2012) Research on permeability improvement and methane driven effect of hydraulic fracturing for low permeability coal seam. Ph.D. thesis, China University of Mining and Technology

Cheng W, Jin Y, Chen M et al (2014) A criterion for identifying hydraulic fractures crossing natural fractures in 3D space. Pet Explor Dev 41:1–6

Cleary MP (1980) Analysis of mechanics and procedures for producing favourable shapes of hydraulic fractures. In: SPE annual technical conference and exhibition, Society of Petroleum Engineers

Daneshy AA (1978) Hydraulic fracture propagation in layered formations. Soc Pet Eng J 18:33–41

Fisher MK, Warpinski NR (2012) Hydraulic-fracture-height growth: real data. Spe Prod Oper 27(1):8–19

Gu H, Weng X, Lund JB et al (2011) Hydraulic fracture crossing natural fracture at nonorthogonal angles: a criterion, its validation and applications. In: Proceedings of SPE hydraulic fracturing technology conference, Society of Petroleum Engineers

Guo T, Zhang S, Qu Z et al (2014) Experimental study of hydraulic fracturing for shale by stimulated reservoir volume. Fuel 128(14):373–380

Huang BX, Liu CY, Fu JH, Guan H (2011) Hydraulic fracturing after water pressure control blasting for increased fracturing. Int J Rock Mech Min Sci 48:976–983

Huang BX, Li PF, Ma J, Chen SL (2014) Experimental investigation on the basic law of hydraulic fracturing after water pressure control blasting. Rock Mech Rock Eng 47:1321–1334

Rutledge J, Yu X, Leaney S et al (2014) Microseismic shearing generated by fringe cracks and bedding-plane slip: Seg Technical Program Expanded, C

Suarez-Rivera R, Burghardt J, Stanchits S et al (2013) Understanding the effect of rock fabric on fracture complexity for improving completion design and well performance. In: SPE international petroleum technology conference, Society of Petroleum Engineers, C

Tada H, Paris PC, Irwin GR (1973) The stress analysis of cracks handbook. Del Research Corporation, Hellertown

Teufel LW, Clark JA (1984) Hydraulic fracture propagation in layered rock: experimental studies of fracture containment. Soc Pet Eng J 24:19–32

Thiercelin MJ, Roegiers JC, Boone TJ et al (1987) An investigation of the material parameters that govern the behavior of fractures approaching rock interfaces. In: Proceedings of 6th ISRM congress, international society for rock mechanics

Warpinski NR, Schmidt RA, Northrop DA (1980) In-situ stresses: the predominant influence on hydraulic fracture containment. J Pet Technol 34:653–664

Warpinski NR, Clark JA, Schmidt RA et al (1982) Laboratory investigation on the-effect of in situ stresses on hydraulic fracture containment. Soc Pet Eng J 22:333–340

Wei F, Ames BC, Bunger AP et al (2016) Impact of partially cemented and non-persistent natural fractures on hydraulic fracture propagation. Rock Mech Rock Eng 49(11):4519–4526

Weng XW (2015) Modeling of complex hydraulic fractures in naturally fractured formation. J Unconv Oil Gas Resour 9:114–135

Zhao HF, Chen M (2010) Extending behavior of hydraulic fracture when reaching formation interface. J Pet Sci Eng 74:26–30

Zhou J, Chen M, Jin Y et al (2008) Analysis of fracture propagation behavior and fracture geometry using a triaxial fracturing system in naturally fractured reservoirs. Int J Rock Mech Min Sci 45:1143–1152

Zhou J, Jin Y, Chen M (2010) Experimental investigation of hydraulic fracturing in random naturally fractured blocks. Int J Rock Mech Min Sci 47:1193–1199

Zou Y, Zhang S, Tong Z et al (2016) Experimental investigation into hydraulic fracture network propagation in gas shales using CT scanning technology. Rock Mech Rock Eng 49(1):1–13